HYDRODYNAMIC DRAG OF A BALL CONTAINING A CONDUCTION-TYPE SOURCE OF ELECTROMAGNETIC FIELDS

V. I. Shatrov and V. I. Yakovlev

UDC 533.9

Investigations were stated in [1] on the influence of electromagnetic bulk forces (EBF) on the flow pattern around and the magnitude of the hydrodynamic drag of a sphere. The EBF was produced by an electromagnetic source of induction type located within the sphere and capable of setting the sphere into translational motion relative to the fluid. From the graphs represented in [1] one interesting result can be noted: that the pressure drag coefficient in the self-moving mode is almost an order of magnitude less than its classical value for all the Reynolds numbers investigated between 50 and 300. It is important to clarify whether this result is random and associated with the operating mode used in [1] when the EBF did not depend on the velocity field under investigation, or it holds for other internal sources. It is also interesting to confirm the hypothesis of the possibility of reducing the total drag coefficient for Re values exceeding 300. To obtain answers to the questions posed, numerical investigations were continued by using a conduction source in the regimes when the electrical field and bulk force distributions in the liquid depend on the velocity field for Reynolds number values of 10^3. This paper is devoted to a description of the results of these numerical experiments. It is shown that the pressure drag in a self-moving regime of internal source operation is a small fraction of the total drag in all the cases considered. It is confirmed that the total drag of a self-moving sphere can be less than its classical value since a 20% drag reduction is obtained in one of the internal source operating modes for Re = 1000. The example of such a flow permits the assertion that the internal source EBF possess the capability of reducing the hydrodynamic drag of small span bodies.

A sphere of radius a is considered with an internal electromagnetic field source in a viscous incompressible fluid flow. The flow velocity at infinity is $\mathbf{u}_0$, the density, kinematic viscosity, and fluid conductivity are ρ, ν, σ, respectively. The internal source consists of a magnetic system and a system of sectioned electrodes producing a magnetic and electric field distribution, periodic in α, within the fluid, and a bulk force distribution associated with these fields. (The spherical coordinates are introduced analogously to [1], in particular, the angle θ is measured from the direction opposite to $\mathbf{u}_0$.)

The magnetic field in a fluid in an induction-free approximation depends only on the magnetic system and is determined uniquely by the assignment of its r-component on the sphere surface. Let

$$H_r|_{r=1} = H_0 h(\theta) \cos m\alpha, \tag{1}$$

where m is the analog of the number of pole-pairs of the magnetic system, the function $h(\theta)$ characterizes the H_r distribution over the sphere surface. We assume that $|h(\theta)|_{max} = 1$, therefore H_0 defines the scale of the magnetic field in the system. The dimensionless magnetic field in the fluid $\mathbf{H}(r, \theta, \alpha) = -\text{grad}\,\chi(r, \theta, \alpha)$ is described by a scalar potential satisfying the Laplace equation and the conditions

$$\partial\chi/\partial r|_{r=1} = -h(\theta) \cos m\alpha, \quad \chi|_{r=\infty} = 0. \tag{2}$$

The solution for χ has the form

$$\chi(r, \theta, \alpha) = \hat{\chi}(r, \theta) \cos m\alpha, \quad \hat{\chi}(r, \theta) = \sum_{l=m}^{\infty} A_l P_l^m(\cos\theta)\, r^{-(l+1)}, \tag{3}$$

where the coefficients

$$A_l = \frac{2l+1}{2(l+1)} \frac{(l-m)!}{(l+m)!} \int_{-1}^{1} h(\theta)\, P_l^m(\cos\theta)\, d\cos\theta$$

Novosibirsk. Translated from Zhurnal Prikladnoi Mekhaniki i Tekhnicheskoi Fiziki, No. 1, pp. 22-28, January-February, 1985. Original article submitted December 19, 1983.

0021-8944/85/2601-0019$09.50

are determined from the first boundary condition in (2).

As already noted, the outer surface of the sphere is comprised of perfectly sectioned electrodes whose dimensionless potential is given in the form

$$\varphi(1, \theta, \alpha) = \varphi_0(\theta) \sin m\alpha. \tag{4}$$

In specific computations $\varphi_0(\theta)$ was taken proportional to the function $h(\theta)$ defining the magnetic field (1) on the sphere surface, in the form

$$\varphi_0(\theta) = -(\varkappa/m)h(\theta), \tag{5}$$

where the parameter $\varkappa$ yields the maximal value of the dimensionless α-component of the electric field on the sphere surface. The potential distribution in the fluid satisfies the equation

$$\Delta\varphi = (\mathbf{H} \cdot \operatorname{curl} \mathbf{v}) \tag{6}$$

and, therefore, depends on the velocity field. Let us note that u_0H_0/c and u_0H_0a/c, the velocity scale u_0 are taken as the scales of the electric field and its scalar potential to make the proceedings dimensionless, while the bulk forces are made dimensionless by using the scale

$$f_0 = \sigma u_0 H_0^2/c^2.$$

We assume that the hydrodynamic flow pattern is axisymmetric

$$\mathbf{v} = v_r(r, \theta)\mathbf{e}_r + v_\theta(r, \theta)\mathbf{e}_\theta, \quad \mathbf{w} = \operatorname{rot} \mathbf{v} = w(r, \theta)\mathbf{e}_\alpha. \tag{7}$$

The potential satisfying (6), the boundary condition (4), and the condition $\varphi|_{r=\infty} = 0$ here has the following solution

$$\varphi(r, \theta, \alpha) = \hat{\varphi}(r, \theta) \sin m\alpha, \tag{8}$$

where $\hat{\varphi}(r, \theta)$ is determined from the problem

$$\begin{gathered} \frac{\partial^2}{\partial r^2}(r\hat{\varphi}) + \frac{1}{r\sin\theta}\frac{\partial}{\partial\theta}\left(\sin\theta\frac{\partial\hat{\varphi}}{\partial\theta}\right) - \frac{m^2}{r\sin^2\theta}\hat{\varphi} = \frac{m}{\sin\theta}\hat{\chi}(r, \theta)w(r, \theta), \\ \hat{\varphi}(1, \theta) = \varphi_0(\theta), \quad \hat{\varphi}(\infty, \theta) = 0. \end{gathered} \tag{9}$$

The following refinement must be made relative to the assumption (7). We start with the remark that the force field

$$\mathbf{f}_1 = [\mathbf{E} \times \mathbf{H}] + (\mathbf{H} \cdot \mathbf{v})\mathbf{H} - \mathbf{H}^2\mathbf{v} \tag{10}$$

is generally nonaxisymmetric for the fields $\mathbf{E}$, $\mathbf{H}$, $\mathbf{v}$ given by the relationships (8), (3), (7). It contains an additional three-dimensional addition dependent on α, i.e., can be represented in the form

$$\mathbf{f}_1 = [f_r(r, \theta)\mathbf{e}_r + f_\theta(r, \theta)\mathbf{e}_\theta] + [\tilde{f}_r(r, \theta)\cos 2m\alpha\mathbf{e}_r + \tilde{f}_\theta(r, \theta)\cos 2m\alpha\mathbf{e}_\theta + \tilde{f}_\alpha(r, \theta)\sin 2m\alpha\mathbf{e}_\alpha]; \tag{11}$$

$$\begin{aligned} f_r &= \frac{1}{2}\left\{-\frac{m}{r^2\sin\theta}\frac{\partial}{\partial\theta}(\hat{\varphi}\hat{\chi}) + \frac{v_\theta}{r}\frac{\partial\hat{\chi}}{\partial r}\frac{\partial\hat{\chi}}{\partial\theta} - \frac{v_r}{r^2}\left[\left(\frac{\partial\hat{\chi}}{\partial\theta}\right)^2 + \left(\frac{m\hat{\chi}}{\sin\theta}\right)^2\right]\right\}, \\ f_\theta &= \frac{1}{2}\left\{\frac{m}{r\sin\theta}\frac{\partial}{\partial r}(\hat{\varphi}\hat{\chi}) + \frac{v_r}{r}\frac{\partial\hat{\chi}}{\partial r}\frac{\partial\hat{\chi}}{\partial\theta} - v_\theta\left[\left(\frac{\partial\hat{\chi}}{\partial r}\right)^2 + \left(\frac{m\hat{\chi}}{r\sin\theta}\right)^2\right]\right\} \end{aligned} \tag{12}$$

(expressions are not presented here for the components of $\mathbf{f}$). Therefore, the desired velocity field can also be represented in the form of a sum $\mathbf{v}_1(r, \theta, \alpha) = \mathbf{v}(r, \theta) + \tilde{\mathbf{v}}(r, \theta, \alpha)$, $(\langle\tilde{\mathbf{v}}(r, \theta, \alpha)\rangle = 0$, where the angular brackets denote the results of taking the average with respect to the angle α), where the first term in the sum, which describes the axisymmetric velocity field component of interest to us, is represented by the equations $\operatorname{div}\mathbf{v} = 0$, $(\mathbf{v}\nabla)\mathbf{v} = -\nabla p + (2/\mathrm{Re})\Delta\mathbf{v} + 2N\mathbf{f} - \langle(\tilde{\mathbf{v}}\nabla)\tilde{\mathbf{v}}\rangle$ containing an axisymmetric component of the force field $\mathbf{f}(r, \theta)$, an axisymmetric component of the pressure $p(r, \theta)$, and additional (Reynolds) stresses due to the three-dimensional addition in the velocity field. Since the solution of the problem in the complete three-dimensional formulation is fraught with almost insuperable difficulties at this time (the three-dimensionality in the presence of large gradients in the desired quantities), there is a need to limit the investigation to the axisymmetric part of the flow by ignoring the mentioned Reynolds stresses in the motion equation. The admissibility of this latter step is confirmed indirectly by using calculations of the component $\tilde{\mathbf{f}}$ (after solving

each variant) and comparing them with the force field $\mathbf{f}$ which takes part in the formation of the axisymmetric velocity field. Calculations show that the components $\tilde{f}_r$, $\tilde{f}_\alpha$ are negligibly small in the versions investigated and they need not be taken into account. As regards $\tilde{f}_\theta$, the fact that although its maximal value (occurring directly at the surface of the sphere at the point $\theta = \pi/2$) is just 2.5-3.0 times smaller than the maximal value of f_θ, and $\tilde{f}_\theta$ damps out much more rapidly both along the radius, and with the distance from the angle $\theta = \pi/2$. It can consequently be expected that three-dimensional additions to the velocity field are considerably weaker than the axisymmetric components. Therefore, the Reynolds stresses they specify are small compared with the term $(\mathbf{v}\cdot\nabla)\mathbf{v}$ in the motion equations, and discarding them does not result in noticeable error in the description of the axisymmetric part of the flow. Precisely this circumstance is indeed to be understood when the assumption (7) is mentioned.

The considerations presented do not naturally avert the necessity for studying the problem in a three-dimensional formulation but permit it to be simplified by making possible the utilization of linearization in the small three-dimensional additions to the velocity field.

Thus, under assumption (7) the problem is reduced to the combined solution of (9) and the hydrodynamics equations in the stream function-vortex variables [1]:

$$E^2\psi - rw\sin\theta = 0,$$

$$-\frac{1}{2r}\left[\frac{\partial\psi}{\partial r}\frac{\partial}{\partial\theta}\left(\frac{w}{r\sin\theta}\right) - \frac{\partial\psi}{\partial\theta}\frac{\partial}{\partial r}\left(\frac{w}{r\sin\theta}\right)\right] + \frac{1}{\mathrm{Re}}\frac{1}{r\sin\theta}E^2(r\sin\theta w) + N\Phi(r,\theta) = 0,$$

where $\Phi = \mathrm{curl}_\alpha \mathbf{f}(r, \theta)$ [the field $\mathbf{f}$ is defined by the relationships (12)], $\mathrm{Re} = u_0 2a/\nu$; $N = \frac{1}{4}\frac{f_0 a}{\rho u_0^2/2}$, and the operator is $E^2 = \frac{\partial^2}{\partial r^2} + \frac{\sin\theta}{r^2}\frac{\partial}{\partial\theta}\left(\frac{1}{\sin\theta}\frac{\partial}{\partial\theta}\right)$.

The numerical solution is performed analogously to [1]. A more compact computational mesh containing 80 points along the radius and 60 points along the angle θ was used on the sphere surface.

The calculations were executed for functions $h(\theta) = \sin^2\theta$ and $\varphi_0(\theta)$ defined by (5) for which the maximal force field is produced near the plane $\theta = \pi/2$. The Reynold number varied between 10^2 and 10^3, the parameter $\varkappa = 1.6$, and the number m took on the values 4 and 10.

The distributions ψ, w, φ and the distribution of the dimensionless bulk forces in the fluid, as well as the pressure distribution on the sphere surface were calculated for different N. As in [1], on the basis of these data the drag coefficients $c_p(N)$, $c_f(N)$, and $c_d(N)$, the dimensionless thrust force

$$F_1(m, N) = -\int_1^\infty\int_0^\pi (f_r\cos\theta - f_\theta\sin\theta)\,2\pi r^2\sin\theta\,d\theta\,dr,$$

as well as the value $N = N_*$ at which the sphere becomes self-moving, were calculated. Also calculated were the magnitudes of the electrical power consumed

$$\sigma\left(\frac{u_0 H_0}{c}\right)^2 a^3\int_1^\infty\int_0^\pi \{[\mathbf{E} + (\mathbf{v}\times\mathbf{H})]\cdot\mathbf{E}\}\,2\pi r^2\sin\theta\,d\theta\,dr,$$

the total mechanical power of the bulk forces

$$f_0 a^3 u_0\int_1^\infty\int_0^\pi (\mathbf{f}\cdot\mathbf{v})\,2\pi r^2\sin\theta\,d\theta dr,$$

and two different efficiencies

$$\eta = \frac{\text{thrust power} = \pi a^2\frac{\rho u_0^2}{2}c_d(N_*)\,u_0}{\text{electrical power}},$$

$$\eta_{\text{prop}} = \frac{\text{thrust power}}{\text{mechanical power}}.$$

The results of calculations of the designated integral quantities, referring to the mode N_*, are presented in Table 1. Presented for comparison in the last column of the table are also

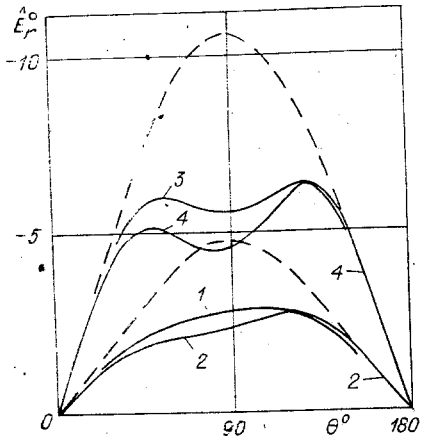

Fig. 1

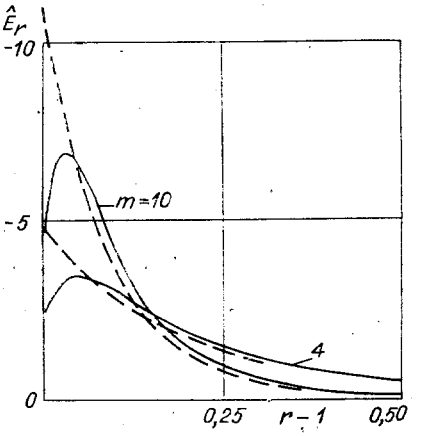

Fig. 2

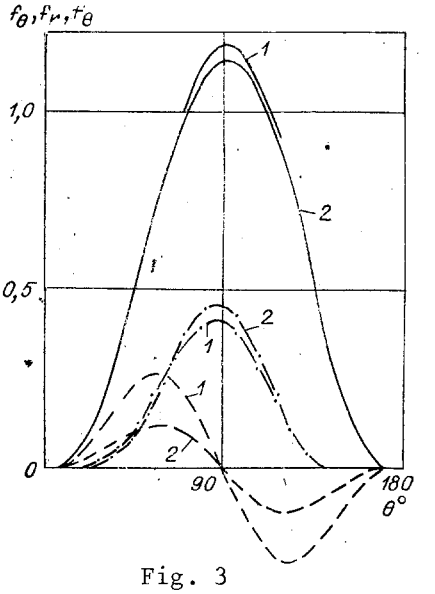

Fig. 3

values of the drag coefficient for a classical flow (N = 0) calculated by means of the formula [2]

$$c_d = \frac{24}{\mathrm{Re}}\left(1 + 0{,}2207\sqrt{\mathrm{Re}} + \frac{\mathrm{Re}}{80}\right),$$

obtained by processing the experimental data for $1 \leqslant \mathrm{Re} \leqslant 1000$.

It is seen from the data presented in Table 1 that in all cases $c_p(N_*)$ has value comprising just several percent of the total drag coefficient $c_d(N_*)$ while the relative weight of the pressure drag in the total drag varies between 0.46 for Re = 100 and 0.58 for Re = 400 for the classical flow, and evidently, to still higher values for larger Re. Hence, it is here possible to speak about the disappearance of the pressure drag for the method of sphere motion under consideration, although it should be emphasized that the friction drag grows here and consequently, the total drag also increases in many cases. This drag increase holds

TABLE 1

	Re	N_*	$c_d(N_*)$	$c_p(N_*)$	$c_f(N_*)$	$F_1(m, N_*)$	$\frac{\eta}{\eta_{\mathrm{prop}}}$	$c_d(0)$
$m=4,\ \varkappa=1{,}6$	100	2,58	2,00	—0,11	2,11	0,607	0,347 1,132	1,070
	200	1,535	1,136	—0,043	1,179	0,581	0,342 1,070	0,795
	300	1,148	0,828	—0,018	0,846	0,566	0,340 1,045	0,686
	400	0,952	0,670	—0,005	0,675	0,554	0,336 1,020	0,625
	600	0,757	0,510	0,010	0,500	0,536	0,335 0,993	0,556
	1000	0,610	0,396	0,041	0,355	0,507	0,329 0,946	0,491
$m=10,\ \varkappa=1{,}6$	100	11,0	3,830	—0,189	4,019	0,273	0,442 1,354	1,070
	400	3,46	1,115	—0,052	1,167	0,254	0,431 1,234	0,625
	600	2,54	0,796	—0,030	0,826	0,246	0,432 1,215	0,556
	1000	1,80	0,540	—0,009	0,549	0,235	0,423 1,137	0,491

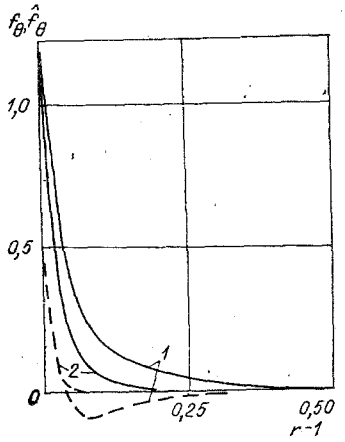

Fig. 4

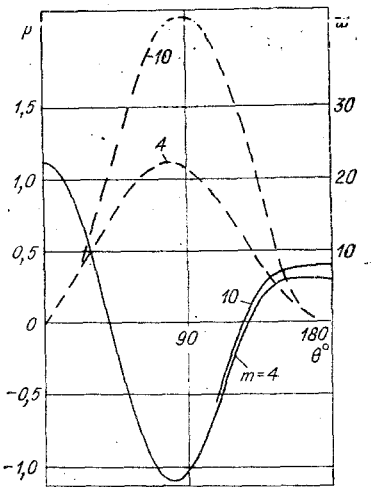

Fig. 5

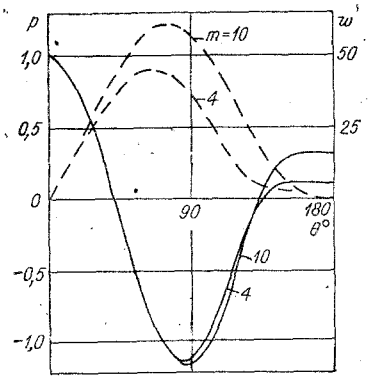

Fig. 6

for smaller values of the Reynolds number and vanishes as Re increases. Let Re_0 be that Reynold number for which the drag of a self-moving sphere equals its classical value; then as is seen from the table, Re_0 lies between 400 and 600 for m = 4, while a diminution in the total drag coefficient of approximately 20% already occurs for Re = 1000. For larger m the increase in the total drag because of the EBF is retained to higher values of Re since the force field is here pressed closer to the body surface, has a larger intensity, and by accelerating the near-wall layer of fluid, increases the velocity gradient on the surface more strongly. For instance, as is seen from the table, for m = 10 the value of Re_0 exceeds somewhat, i.e., no diminution in $c_d(N_*)$ as compared with c (0) occurs within the limits $10^2 \leqslant Re \leqslant 10^3$.

The value of the efficiency varies, in the case under consideration, between 0.33 and 0.44, i.e., has a considerable magnitude even for a nonoptimal source. As regards η_{prop}, its magnitude is close to or exceeds one. The system with a free field thereby differs from a channel type propulsion apparatus.

The distributions of the field quantities are given in Figs. 1-6 for certain of the regimes presented in Table 1. The curves in Fig. 1 describe the distribution of the radial electric field component $E_r|_{r=1} = -\partial\hat{\varphi}/\partial r\,|_{r=1} \sin m\alpha = \hat{E}_r^0 \sin m\alpha$ on the sphere surface. Curves 1 and 2 are obtained for m = 4 and Re = 100 and 1000, curves 3 and 4 are obtained for m = 10 and Re = 100 and 1000. Displayed here for comparison by dashed lines are curves for m = 4 and 10 obtained without taking account of the space charge, i.e., curves describing the distribution $E_r|_{r=1}$ in a fixed fluid. It is seen that the volume charge considerably diminishes the normal electric field component near the sphere surface in the area of the equatorial plane $\theta = \pi/2$, where the bulk charge density is maximal. The nature of the change in E_r with distance from the sphere surface is shown in Fig. 2, illustrating the dependence $\hat{E}_r = -\partial\hat{\varphi}/\partial r$ (here the dashed lines also correspond to functions obtained without taking account of the space charge). It is seen that the space charge makes this dependence nonmonotonic. The curves of Fig. 2 correspond to Re = 1000; the results for Re = 100 differ negligibly from those represented on the graph and are not superposed.

This latter remark also refers to Figs. 3 and 4, which characterize the bulk force distribution in the fluid and are constructed for Re = 1000. Given in Fig. 3 is the distribution of the force components from (11) on the sphere surface. Here the solid lines correspond to f_θ, the dashes to f_r, the dash-dots to $\tilde{f}_\theta$, and the numbers 1 and 2 refer, respectively, to m = 4 and 10. Of the components of the field $\tilde{\mathbf{f}}$ describing the three-dimensional addition to the force field (11), only $\tilde{f}_\theta$ is presented since $\tilde{f}_r$, $\tilde{f}_\alpha$ are negligibly small. Their maximal absolute values (from the computational results), achieved at the points $\theta \approx 30$ and 66°, respectively, equal $2.2 \cdot 10^{-3}$ and $4.6 \cdot 10^{-2}$ for m = 4 and are still less for m = 10. Figure 4 illustrates the nature of the drop in f_θ (solid curves) and $\tilde{f}_\theta$ (dashed lines) along the radius in the plane $\theta = \pi/2$ (the numbers 1 and 2 are as in Fig. 3). It is seen that damping of $\tilde{f}_\theta$ occurs considerably more rapidly than of f_θ, where for m = 4 $\tilde{f}_\theta$ does not drop monotonically.

Represented in Figs. 5 and 6 are the pressure (solid lines) and vorticity (dashed lines) distributions in the self-moving mode, respectively, for Re = 100 and 1000. It is seen that the flow is separation-free in all cases and is characterized by the presence of large positive values of the vorticity on the whole sphere surface; the qualitative behavior of the curves is completely analogous to that obtained in [1].

LITERATURE CITED

1. V. I. Shatrov and V. I. Yakovlev, "Change in the hydrodynamic drag of a sphere set in motion by electromagnetic forces," Zh. Prikl. Mekh. Tekh. Fiz., No. 6 (1981).
2. C. L. Lin and S. C. Lee, "Transient state analysis of separated flow around a sphere," Comput. Fluids, 1, No. 3 (1973).

LOCALLY THREE-DIMENSIONAL LAMINAR FLOWS

V. V. Bogolepov and I. I. Lipatov

UDC 532.526

Local variations in the flight vehicle surface, either specially designed or natural, may significantly affect heat transfer and skin friction and determine the state of the boundary layer. Analysis of the limiting solutions to Navier–Stokes equations as $\mathrm{Re} \to \infty$ (Re is Reynolds number) carried out in [1, 2] showed that different states of laminar boundary layer are possible near two-dimensional roughnesses, characterized by a difference in the ratio of viscous forces to inertia forces and in the nature of viscous-inviscid interaction near the roughness. The method of matched asymptotic expansions was used in [1, 2] to study such flow situations and numerical results for the corresponding boundary-value problem were obtained. Subsequently, results were obtained for studies on specific flow conditions or roughness shapes [3-9]. In practice, three-dimensional and not two-dimensional roughness is more frequently encountered; interest in the study of flow past such roughness is also associated with the problem of the flow past elements of relief on the earth's surface. Results of investigations on flow past three-dimensional roughness are given in [10-16]. However, not all possible flow conditions near three-dimensional roughness have been investigated. This paper deals with studies on the flow past roughness whose length is less or equal to the boundary-layer thickness as well as longer roughness in whose neighborhood there is no interaction with the external inviscid flow.

1. Consider a steady flow past three-dimensional roughness located at the bottom of a laminar boundary layer at a distance l from the leading edge of a flat (Fig. 1).

The coordinate system is chosen such that x axis is in the direction of the external flow, y axis is normal to the surface, and z axis is perpendicular to x and y axes. It is assumed that the velocity profile in the laminar boundary layer upstream of the roughness has velocity components in the x and y directions only.

The above assumption is true if the lateral edge of the flat plate is sufficiently far from the roughness. The following notations are used for Cartesian coordinates and the respective vector components of velocity, total enthalpy, density, pressure, and dynamic viscosity:

$$xl,\ yl,\ zl,\ u_\infty u,\ u_\infty v,\ u_\infty w,\quad u_\infty^2 H,\ \rho_\infty \rho,\ \rho_\infty u_\infty^2 p,\ \mu_\infty \mu$$

(the subscript ∞ denotes dimensional quantities in the free stream). Limiting flow situation at large but subcritical Reynolds numbers ($\mathrm{Re} = \rho_\infty u_\infty l/\mu_\infty$) when laminar flow is retained is considered.

It is assumed that the transverse dimension b of the roughness is of the same order as the streamwise dimension a [the flow near slender roughness $b = o(a)$ will be considered below]. It is worth mentioning that the flow past roughness with $a = o(b)$ reduces to a two-dimensional problem and the flow past roughness with equal streamwise and transverse dimensions leads to a three-dimensional problem. It is also assumed that for given values of a and b the thickness of the roughness c is such that in the disturbed flow near the roughness the order of the viscous force is not less than the inertial force. Considering the velocity profile in the boundary layer near the surface of the body to be $u \sim y/\delta_0$ and making an order of magnitude analysis of terms representing viscous and inertial forces in the x-momentum equation, we get

$$c \leqslant O(a\varepsilon^{1/3}),\ \delta_0 = \varepsilon = \mathrm{Re}^{-1/2}. \tag{1.1}$$

Moscow. Translated from Zhurnal Prikladnoi Mekhaniki i Tekhnicheskoi Fiziki, No. 1, pp. 28-36, January-February, 1985. Original article submitted September 19, 1983.

 0021-8944/85/2601-0024$09.50